doi: 10.5028/jatm.v8i1.514

Integration Analysis of Conceptual Design and Stealth-Aerodynamic Characteristics of Combat Aircraft

Cheng Liangliang[1,3], Yue Kuizhi[1,2], Guo Weigang[2], Yu Dazhao[2]

ABSTRACT: In order to study stealth strike-fighter, an analysis on stealth-aerodynamic integration and conceptual design is conducted. A conceptual 3-D digital model with internal antiship missiles and air-to-air missiles is designed in CATIA software. Based on the physical optics and equivalent electromagnetic current methods, using the self-programmed RCSAnsys software, the Radar Cross Section (RCS) characteristics and characteristics of scattering intensity distribution of the model are numerically simulated. Based on the turbulence theory of standard k-ε equations, using Fluent software, the pressure, velocity and lift-to-drag characteristics of the conceptual aircraft are numerically simulated. The simulation results show that the stealth and aerodynamic characteristics of the conceptual aircraft can be designed through integration analysis process, which can provide technical support to the design of the advanced operational aircrafts.

KEYWORDS: Conceptual design, Stealth, Strike-fighter, Computational fluid dynamics, Simulation.

INTRODUCTION

Stealth operational aircraft is one of the trends of the development of modern military aircrafts. Depending on the stealth characteristics of the aircraft, the radar detection probability is reduced, aircraft survivability is enhanced and then the operational function is improved. For that reason, stealth operational aircrafts are under vigorous research and development, such as B-2 (Scott 2006), F-22 (Anonymous 2009), F-35 (Starosta 2013), X-45 (Wise and Lavretsky 2011) and X-47 (Zhang *et al.* 2009) of the USA, stealth T-50 of Russia etc.

Stealth aircraft has been studied throughly by researchers at home and abroad in several respects. Many academic results have been achieved in aircraft conceptual design, the Radar Cross Section (RCS) algorithm and stealth-aerodynamic analysis etc. In Deng and Yu (2013), the conceptual configuration parameters of all-wing aircrafts are discussed. In Yue *et al.* (2014a), the influence of symmetrical incline of double-vertical fins on RCS characteristics is studied based on the physical optics method. In Yue *et al.* (2014b), the RCS characteristics of the aircraft are numerically simulated based on the physical optics and equivalent electromagnetic current methods, and the RCS characteristics of the aircraft are analyzed comparatively between when it is armed with external weapons and with internal weapons. In Saha and Majumdar (2012), the aerodynamic characteristics of delta wing are theoretically simulated at 65° leading edge sweepback angle and a subsonic velocity. Kazuhiro (2013) discusses the application of unstructured mesh in Computer Fluid Dynamics (CFD) aviation. In Vallespin *et al.* (2012), the flight dynamic performances of jet trainers and Unmanned Combat Air

1.Beijing University of Aeronautics and Astronautics – School of Aeronautic Science and Engineering – Department of Airborne Vehicle – Beijing – China. **2.**Naval Aeronautical and Astronautical University – Department of Airborne Vehicle Engineering – Laboratory of Aircraft – Yantai – China. **3.**Naval Aviation Institute – Department of Carrier-based Engineering – Laboratory of Aviation Maintenance – Huludao – China.

Author for correspondence: Yue Kuizhi | Beijing University of Aeronautics and Astronautics – School of Aeronautic Science and Engineering – Department of Airborne Vehicle | Beijing 100191 – China | Email: yuekuizhi_2000@sohu.com

Received: 07/10/2015 | **Accepted:** 02/15/2016

Vehicle (UCAV) are estimated using CFD method. In Peng and Jinglong (2012), the intercoupling theory of CFD and computational structural dynamics (CSD) is applied to discuss wing flutter problem and analyze the aerodynamic and structural properties of the wings with winglets of cargo planes. He *et al.* (2009) studied the numerical simulation of stealth-aerodynamic integration of flying-wing. Although several respects in the domain have been over-studied by researchers at home and abroad, certain problems still need to studied. No public academic reports on stealth strike-fighters have been obtained, and there is a lack of deep research in stealth-aerodynamic integration of conceptual aircrafts.

Aiming at the issue mentioned above, this article conceptually designs the operational aircraft and analyzes the stealth-aerodynamic characteristics of the aircraft. It is expected that the results of the research will provide reference basis and technical support to the conceptual and stealth design of the aircraft.

CONCEPTUAL DESIGN

The strike-fighter conceptually designed in the article is a kind of operational aircraft with a single seat, double vector engines and normal configuration (Table 1). The layout of the conceptual strike-fighter is as follows: a pair of flaperons, a pair of fore flaps, a pair of moveable strake wings, canted double-vertical stabilators, a pair of differential tailplanes, blended wing body configuration, tricycle landing gears, a internal weapon bay, and four hardpoints under the main wings. The 3-D digital prototype of the conceptual strike-fighter is designed with CATIA software, including digital prototype, a sketch map of the weapon mounting scheme and basic parameters (Fig. 1).

Table 1. Basic parameters of the conceptual strike-fighter.

Parameter	Size
Length	22 m
Height	6.05 m
Span	14.2 m
Leading edge sweepback angle	45°
Trailing edge sweep forward angle	16°
Wingtip chord	1.865 m
Root chord	11.085 m
Canted fin angle	28°
Engine number	2
Airfoil main wing profile	NACA64a204
Airfoil horizontal wing profile	NACA64a202
Airfoil fin profile	NACA64a003

The weapon mounting scheme is shown in Fig. 2 as follows: (a) Scheme 1, the aircraft carries an internal long-range supersonic antiship missile and executes antiship missions; (b) Scheme 2, the aircraft carries 2 × 5 internal mid-range air-to-air missiles and executes air battle missions; (c) Scheme 3, the aircraft carries a mid-range supersonic antiship missile and five mid-range air-to-air missiles as well as executes antiship and air battle missions.

After the conceptual design, the RCS characteristics and aerodynamic characteristics are numerically simulated so that the stealth-aerodynamic performance can be analyzed.

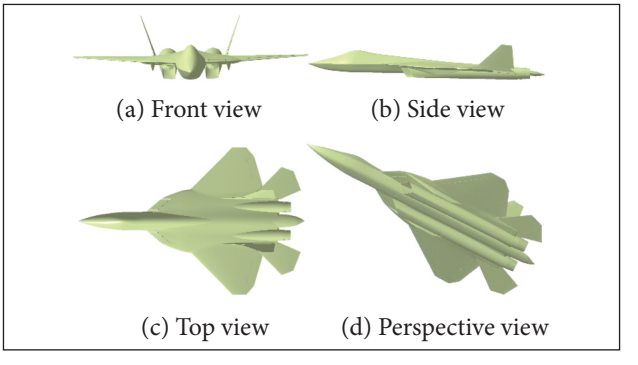

Figure 1. 3-D digital prototype.

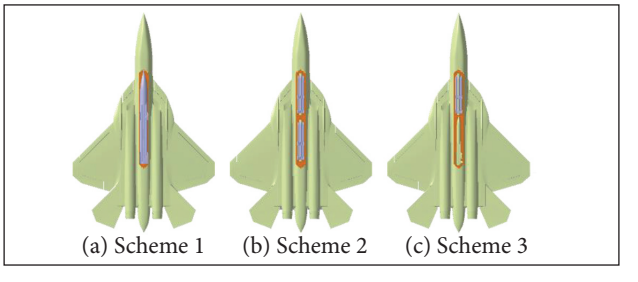

Figure 2. Diagram of the aircraft with missiles.

THEORETICAL BASIS

The theoretical basis of stealth and aerodynamics of combat aircraft includes three parts: the testing algorithm of RCS, the theoretical basis of CFD, and the process of analysis of the stealth-aerodynamic integration.

TESTING ALGORITHM OF RCS

Two respects are usually considered in stealth performance: radar stealth and infrared stealth. The article only analyzes the

RCS characteristics of the aircraft for it is the main characteristic in the stealth domain.

Regardless camouflage paint, when looking at the geometric profile of an aircraft, the testing algorithms for the numerical simulation of RCS characteristics are the physical optics and equivalent electromagnetic current methods. The surface element scattering is calculated by the former method, and the edge diffraction is calculated by the latter (Baussard *et al.* 2011; Rochdi *et al.* 2010).

The equation of the physical optics method is:

$$\sqrt{\sigma_{po}} = -j\frac{k}{\sqrt{\pi}}\int_s \vec{n}\cdot(\vec{e}_r \times \vec{h}_i)\exp[jk\vec{r}(\vec{i}-\vec{s})]\mathrm{d}S \qquad (1)$$

where: $\sqrt{\sigma_{po}}$ (in m²) is the RCS of a single surface element; j is the imaginary unit and $j^2 = -1$; $k = 2\pi/\lambda$ is the free space wave beam, where λ (in m) is the length of incoming radar wave; s is the surface exposed to radar; $\vec{n}$ is the unit normal vector of object surface; $\vec{e}_r$ is the unit vector at the electromagnetic direction of receiving antenna; $\vec{h}_i$ is the unit vector of the direction of the incoming wave field; $\cdot$ is the dot product; $\times$ is the cross product; $\vec{r}$ is the vector from local origin to surface unit dS; $\vec{i}$ is the unit vector of the incoming direction; $\vec{s}$ is the unit vector of scattering direction.

The equation of equivalent current method is:

$$\sqrt{\sigma_{ecm}} = \frac{1}{\sqrt{\pi}\sin\theta}[(\vec{E}_o^i\cdot\vec{t})f\vec{s}\times(\vec{s}\times\vec{t}) - Z_0(\vec{H}_0^i\cdot\vec{t})g\vec{s}\times\vec{t}]\cdot e^{-j2k\vec{r}_t\cdot\vec{s}}\frac{\sin(k\vec{l}\cdot\vec{s})}{k\vec{l}\cdot\vec{s}} \qquad (2)$$

where: $\sqrt{\sigma_{ecm}}$ (in m²) is the RCS of a single edge; $\vec{t}$ is the tangential unit vector of the edge; q is the angle between incoming waves $\vec{i}$ and $\vec{t}$; $\vec{E}_o^i$ (in V/m) is the intensity of incoming electric field; f and g are Ufimtsev diffraction coefficients; Z_0 (in Ω) is the impedance of vacuum wave; $\vec{H}_o^i$ (in A/m) is the incoming magnetic field intensity; $\vec{r}_t$ is the middle-position vector of the edge; $\vec{l}$ is the edge vector.

The RCS of the strike-fighter is the total of the RCS of n surface units and m edges. The superposition equation is:

$$\sigma = \left|\sum_{i=1}^{n}(\sqrt{\sigma_{po}})_i + \sum_{j=1}^{m}(\sqrt{\sigma_{ecm}})_j\right|^2 \qquad (3)$$

The arithmetic mean value of RCS of the fighter is:

$$\bar{\sigma} = \frac{1}{N}\sum_{i=1}^{N}\sigma_i \qquad (4)$$

The RCS unit conversion of the fighter is:

$$\sigma_{dBsm} = 10\lg_{10}\sigma \qquad (5)$$

where: σ (in m²) is the RCS of the fighter; $\bar{\sigma}$ is the RCS arithmetic mean; σ_{dBsm} (in dBsm) is the RCS of the fighter.

THEORETICAL BASIS OF CFD

The turbulence numerical simulation theory of the conceptual strike-fighter adopts the standard k-ε equations, which are:

$$\frac{\partial(\rho k)}{\partial t} + \frac{\partial(\rho k u_i)}{\partial x_i} = \frac{\partial}{\partial x_j}\left[(\mu + \frac{\mu_t}{\sigma_k})\frac{\partial k}{\partial x_j}\right] + G_k + G_b - \rho\varepsilon - Y_M + S_k \qquad (6)$$

$$\frac{\partial(\rho\varepsilon)}{\partial t} + \frac{\partial(\rho\varepsilon u_i)}{\partial x_i} = \frac{\partial}{\partial x_j}\left[(\mu + \frac{\mu_t}{\sigma_\varepsilon})\frac{\partial\varepsilon}{\partial x_j}\right] + C_{1\varepsilon}\frac{\varepsilon}{k}(G_k + C_{3\varepsilon}G_b) - C_{2\varepsilon}\rho\frac{\varepsilon^2}{k} + S_\varepsilon \qquad (7)$$

where: ρ is fluid density; k is the turbulent kinetic energy; t is the time; u_i is the speed per time; μ is the viscosity of fluid power; μ_t is the turbulent viscosity; σ_k is the Prandtl number corresponding to the turbulent kinetic energy k; G_k is the production of turbulent kinetic energy caused by the average velocity gradient; G_b is the production caused by the buoyancy of the turbulent kinetic energy; $\boldsymbol{\varepsilon}$ is the turbulent dissipation rate; Y_M is the contribution to the expansion of pulsation in the turbulence; S_k is the source term defined by users; σ_ε means the Prandtl number corresponding to dissipation rate; $C_{1\varepsilon}$, $C_{2\varepsilon}$ and $C_{3\varepsilon}$ are the empirical constants; S_k is the source term defined by users.

The RANS method is applied to solve the turbulent flow problem.

The standard k-$\boldsymbol{\varepsilon}$ model is applied to turbulence model with high Reynolds number (Re) values while the wall-function method is adopted to solve the model with low Re values.

The wall-function method which contains a set of semi-empirical formulae is used to refine the near-wall region.

$u^+ = 1/k\ln(Ey^+)$ and $y^+ = \Delta y_p(C_\mu^{1/4}k_p^{1/2})/\mu$ are derived, where $y^+ > 11.63$ on the control node near the wall.

$u^+ = y^+$ and $y^+ = \Delta y/\nu\sqrt{\tau_w/\rho}$ are derived, where $y^+ < 11.63$ on the control node near the wall.

where: y^+ is a non-dimensional parameter and $y^+ = \Delta y \rho u_\tau / \mu$; Δy is the distance to the wall; $u_\tau = (\tau_w / p)^{1/2}$ is the wall friction velocity and τ_w is the wall shear stress; u^+ is a non-dimensional parameter and $u^+ = u/u_\tau$; u is the mean velocity of the fluid; E is the energy of the fluid; Δy_p is the distance from node p to the wall; C_μ is an empirical constant and k_p is the kinetic energy of node p.

THE ANALYSIS PROCESS OF THE STEALTH-AERODYNAMIC INTEGRATION

The main steps for analysis of the stealth-aerodynamic integration are as follows. A 3-D model of the aircraft is built in CATIA software; (2) with the self-compiled software named RCSAnsys, the RCS of the model is numerically simulated based on physical optics and equivalent electromagnetic current methods; (3) the CFD numerical simulation of the model is conducted with Fluent software; (4) the performances of stealth-aerodynamic integration of the model will be analyzed comprehensively. The model of the aircraft should be improved or rebuilt until the results meet the demands.

After the theoretical basis is obtained, the analysis and simulation are conducted as follows.

RESULTS AND DISCUSSION

There are two parts in this section: the results and discussion of RCS and the results and discussion of CFD.

RCS

Based on the physical optics and equivalent electromagnetic current methods, it was used the self-programmed RCSAnsys software to make numerical simulation on the RCS characteristics of the 3-D digital prototype.

The RCS numerical simulation method applied in the paper is an approximate method for cavity calculation, and the exact solution for the inlets and nozzles cannot be obtained. The engines that have not been exposed to radar wave directly for the inlets are closed with inclined protective screening. The inlets of the model are also sealed with inclined planes for the calculation of RCS. The nozzles of the model are closed with cones and annuluses for calculation.

The conditions for the simulation in this paper are: two ways of polarization: H-H and V-V polarization; three pitch angles of incoming radar waves: −5°, 0° and +5°; four frequency bands: L, S, C and X. With Eqs. 1 to 5, the RCS of the plane is numerically simulated and the RCS characteristic curves of 24 planes and 8,640 pictures of RCS scattering feature are obtained.

Under H-H polarization and 0° pitch angle, RCS characteristic curves of frequencies equal to 1.5, 3, 6 and 10 Hz are numerically simulated, as shown in Fig. 3. The RCS mean characteristics are simulated and shown in Tables 2–4. The RCS scattering characteristics of various parts of the plane are obtained, as shown in Fig. 4.

On the one hand, the RCS value of the model in specific direction can be as low as −40 dBsm, which is a very low value shown in Fig. 3 and Tables 2–4; on the other hand, the relatively higher RCS value can be obtained in certain forward angle range of the model. The mean RCS value in a range of ± 30° of the forward direction is −5.625 dBsm when exposed to 10-GHz radar wave. In general, it is the same or even exceeds the stealth level of modern fighters in the world.

The distribution of RCS scattering characteristics of the conceptual strike-fighter is shown in Fig. 4: (a) in the

Table 2. Pitch angle of −5 ° and azimuth range of ± 30° — RCS mean value (in dBsm).

Frequency (GHz)	Polarization type	Front	Side	Back
1.5	HH	−4.040	15.220	−1.834
	VV	−3.971	15.214	−1.839
3	HH	−4.657	18.598	−1.679
	VV	−3.971	15.214	−1.839
6	HH	−2.585	16.492	−0.580
	VV	−2.583	16.484	−0.585
10	HH	−4.943	14.611	−0.927
	VV	−4.952	14.604	−0.927

forward direction, RCS intensity distribution is fairly high on the engine in the air inlet, so there should be measures taken in the entrance of the inlet to reduce the intensity on the engine; (b) in both sides, the RCS intensity in the nose, the body, the air inlet and the tail cone is high; (c) in the backward side, the intensity of the engine is high; (d) under 0° pitch angle of the incoming radar wave and 10° azimuth, the intensity in the front edge of the strake wings and canopies is relatively high; (e) under −5° pitch angle of the incoming radar wave and 170° azimuth, the RCS intensity in the jet nozzle of the engine and in the tail is high; (f) under 10° pitch angle of incoming radar wave and 75° azimuth, the intensity in nose, middle body, tail cone, the air inlet and vertical tailsis high and measures should be taken to reduce the intensity.

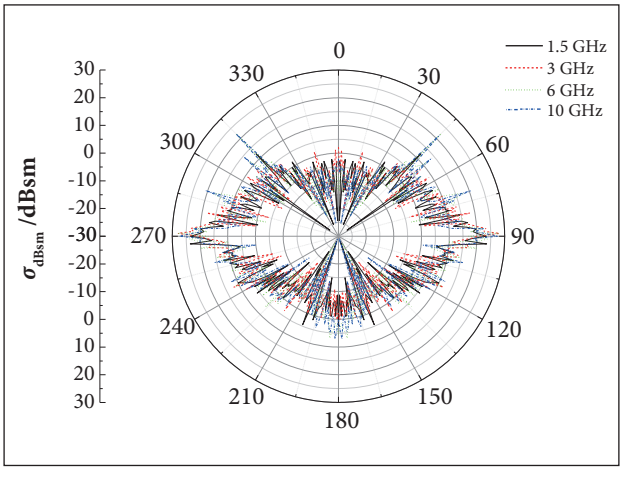

Figure 3. RCS characteristic curves (H-H polarization, pitch angle = 0°).

The numerical simulation of RCS characteristics can be used to calculate the RCS of each component of a plane and understand the RCS scattering characteristics there. It is significant for the further improvement of the forms and structures of the plane and reduction of its RCS intensity.

Next, there is the analysis on the aerodynamic characteristics after the stealth characteristics.

Table 3. Pitch angle of 0° and azimuth range of ± 30° — RCS mean value (in dBsm).

Frequency (GHz)	Polarization type	Front	Side	Back
1.5	HH	−6.056	13.070	−1.374
	VV	−6.197	13.102	−1.496
3	HH	−4.596	15.010	−1.735
	VV	−4.615	15.010	−1.796
6	HH	−7.991	15.248	−0.224
	VV	−8.021	15.238	−0.196
10	HH	−7.982	14.737	−0.140
	VV	−8.003	14.737	−0.133

Table 4. Pitch angle of 5° and azimuth range of ± 30° — RCS mean value (in dBsm).

Frequency (GHz)	Polarization type	Front	Side	Back
1.5	HH	−3.520	8.991	−0.449
	VV	−3.687	8.961	−1.058
3	HH	−5.589	13.885	−0.571
	VV	−5.663	13.859	−0.695
6	HH	−4.922	13.077	0.423
	VV	−4.963	13.098	0.444
10	HH	−5.625	13.542	0.970
	VV	−5.708	13.562	0.951

CFD

It was used ANSYS14.5 software and the Fluent module in the Workbench software so that a CFD analysis was carried out on the conceptual strike-fighter, which mainly includes the following several parts: mesh generation, CFD numerical simulation and lift-drag characteristics analysis.

Mesh Generation

An analysis of the fluid mechanics of the strike-fighter is done. First, the 3-D digital prototype of the plane space is closed. Then we import the Workbench module in the Fluent software. In the Geometry, submodule generates geometric form of the strike-fighter. Then the geometric form is placed on the flow field; then, in the Mesh module, the mesh is generated. The region near the wall is refined with unstructured tetrahedron grid.

The specific processing of the wall function is as follows: the velocity values present a linear distribution along the normal direction of the wall where $y^+ < 11.63$ for the corresponding layer is the viscous sublayer. In this case, $u^+ = y^+$.

The log-law distribution of velocity is observed on normal direction of the wall where $11.63 < y^+ < 300$ for the flow is in log-law layer and $u^+ = 1/\kappa \ln y^+ + B = 1/\kappa \ln(Ey^+)$, where κ is Karman constant, B and E are constants connected with surface roughness and $\kappa = 0.4$, $B = 5.5$ and $E = 9.8$ for smooth surface.

A non-structural mesh of the plane is generated in Mesh module, shown in Fig. 5. The number of grids of the plane in the flow field is 39,686,281.

CFD Numerical Simulation and Lift-Drag Characteristics Analysis

In this section, using Fluent module in Workbench software, the aerodynamic characteristics of the conceptual strike-fighter are numerically simulated. Turbulence numerical simulation theory of the plane uses the standard k-ε equation. As the velocity is 270 m/s and air flow has significant compressibility, the density-based solver is adopted.

Using Fluent software, setting the pressure of the incoming flow at 101,325 Pa, when the coming flow angle is 0°, CFD numerical simulation obtains: pressure distribution on the conceptual strike-fighter surface, as shown in Fig. 6; velocity distribution of flow field of the conceptual strike-fighter, as shown in Fig. 7.

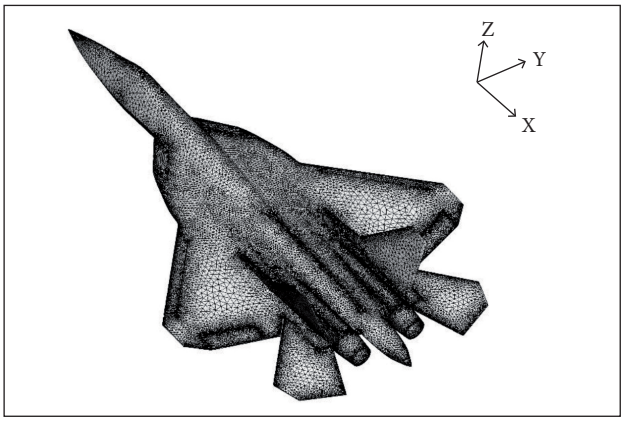

Figure 5. Grids of the conceptual strike-fighter.

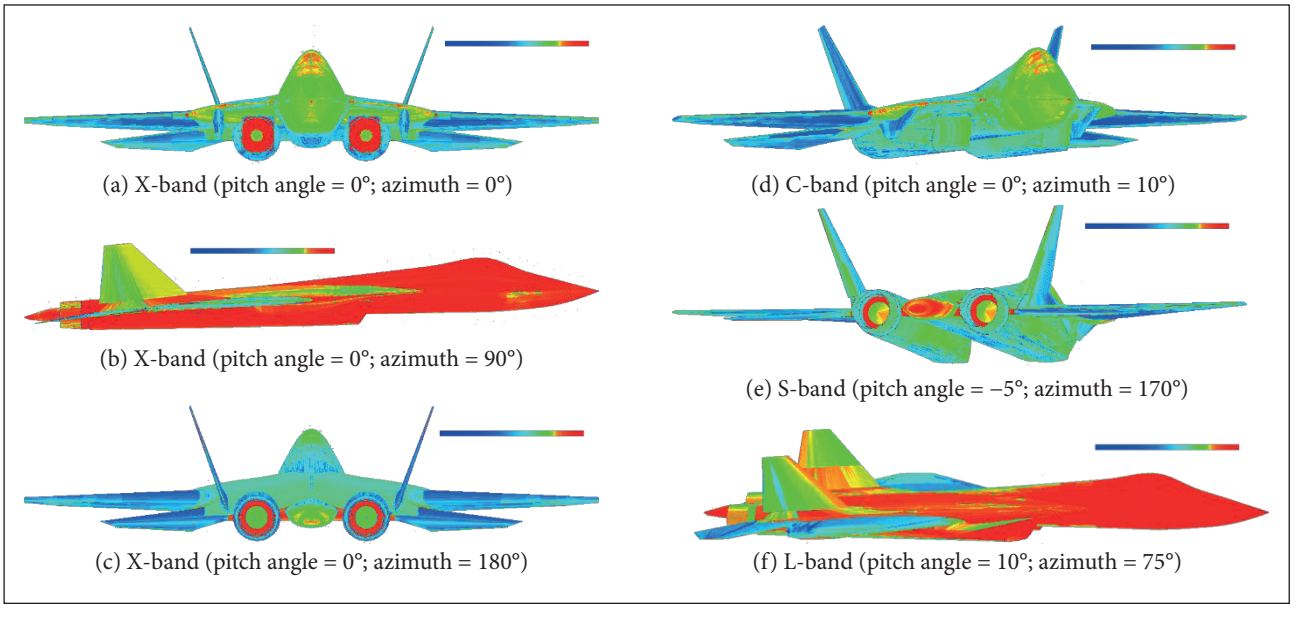

Figure 4. RCS scattering properties of aircraft components.

Figure 6 shows the distribution of pressure on the upper and bottom surfaces of the plane. Figure 6a shows that: the pressure on the upper plane surface is small; the plane nose pressure is strong and radome frontal pressure is greater than 1.2×10^5 Pa; pressure on the aircraft canopy and on the wing leading edge is smaller, and the minimum is 8.679×10^4 Pa; the greatest pressure is on the horizontal tail wing surface, near the 9.714×10^4 Pa; the tail cone rear pressure is strong, where the maximum pressure is about 1.2×10^5 Pa.

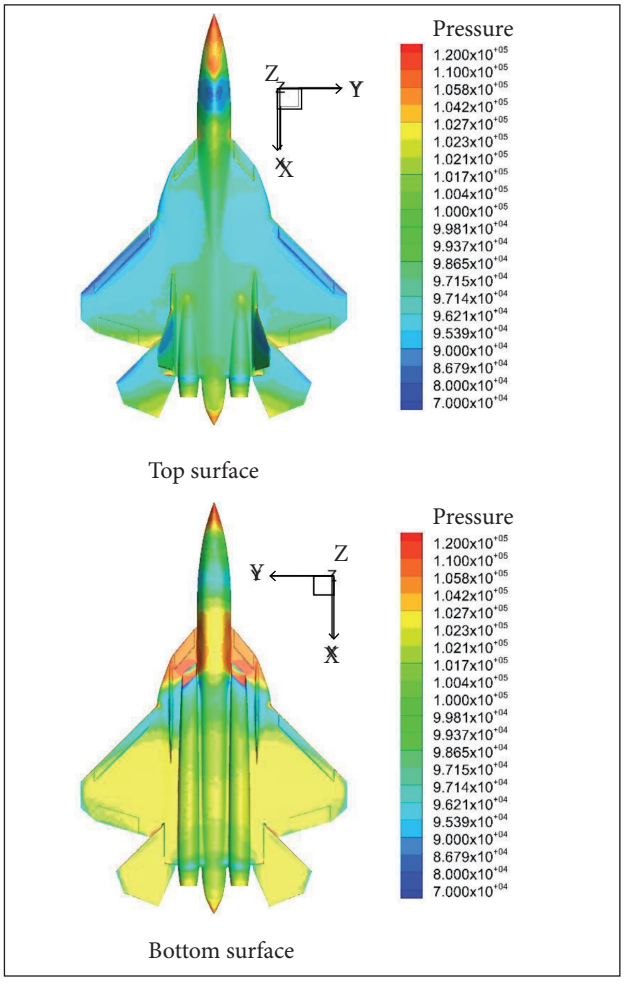

Figure 6. Pressure distribution of the conceptual strike-fighter.

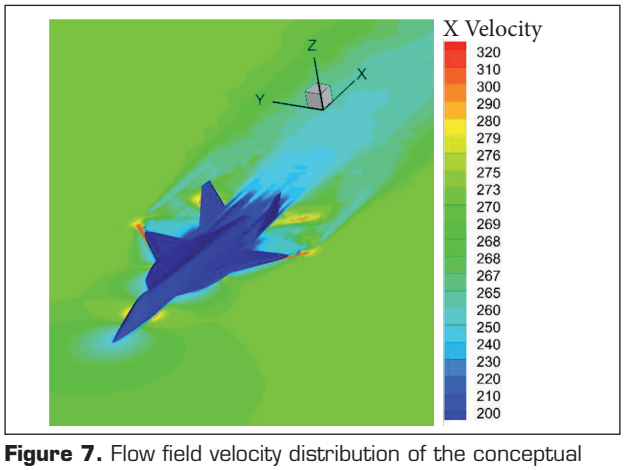

Figure 7. Flow field velocity distribution of the conceptual strike-fighter.

It is known from Fig. 6b that: the bottom surface of the plane is under higher pressure; the pressure on the bottom surface is higher than that on the top surface of the forward part of the plane body, the effect of which provides a lift for the plane; on the fuselage, bottom surface and the top surface have similar pressure. The bottom surface of the middle part contributes with a small part to the lift force; on the backward fuselage, the bottom surface is under stronger pressure than on the top surface, about 1.021×10^5 Pa, and the bottom surface of backward body has a contribution to the lift; the wings, flat tail and moving strake wings are under stronger pressure on the bottom surface than on the top surface pressure, and the lower pressure is about 1.027×10^5 Pa. The wings, flat tail and movable strake wings all contribute to the lift force.

Under the coming flow velocity of 270 m/s and the pitch angle of 0°, in x-y plane, the aircraft and its surrounding air flow field velocity distribution is shown in Fig. 7: in x-y plane, the incoming wave velocity is axisymmetric along x axis; the front of the nose, movable strake wings and main wings have a small flow speed, the minimum of which is less than 200 m/s; air flow is slow behind the rear fuselage and the back of wings, and flow separation phenomenon is observed. Low speed air flow area is longer than the others; on both sides of the nose cockpit and airplane wing tips, the air velocity is larger, and in some parts it is more than 290 m/s.

The distribution of pressure and velocity of the case as well as the lift-drag characteristics of the aircraft are obtained through CFD numerical simulation in Fluent software under the following conditions: the pressure of incoming flow from the distant flow field is 101,325 Pa, the incoming flow velocity is 270 m/s and the pitch angle is in a range of −6° to +15°. The simulation results are shown in Table 5.

A total of eight simulations are conducted in Fluent software with angles of attack at −6°, −3°, 0°, 3°, 6°, 9°, 12° and 15°, respectively, to obtain the lift and drag coefficients

Table 5. Lift-drag characteristics.

Angle of attack (°)	Lift-drag characteristics		
	Lift coefficient	Drag coefficient	Lift-drag ratio
−6	−0.1313	0.0373	−3.5201
−3	0.0239	0.0349	0.6848
0	0.1732	0.0389	4.4524
3	0.3277	0.0485	6.7567
6	0.4976	0.0801	6.2122
9	0.6837	0.1535	4.4540
12	0.8568	0.1969	4.3514
15	1.0866	0.3159	3.4396

and lift-drag ratios. The CFD simulation converges after about 6,000 steps of calculation; then the convergence property of the simulations is verified and the results at different angles of attack are also obtained.

A CFD numerical simulation of the aerodynamic characteristics of the plane cannot obtain the distribution of pressure and velocity of the plane as well as analyze the lift-drag characteristics so as to evaluate aerodynamic designs of the conceptual aircraft.

The integrated design and analysis of stealth and aerodynamics are embodied in the process of parametric variation study. The parameters are changing until they meet the design requirements. The satisfied parameters are obtained through iterating in integrated analysis and the process of analysis on stealth-aerodynamic integration is presented in this paper.

CONCLUSION

In the present research, the advanced combat aircraft is conceptually designed, and its stealth-aerodynamic characteristics are analyzed, reaching the following conclusions:

- The design and analysis of the stealth-aerodynamic characteristics of the conceptual aircraft can be based on the analysis process of the integration of stealth aircraft conceptual design and aerodynamic analysis.
- Under V-V polarization, the mean RCS of forward ± 30° part of the plane is $\overline{\sigma}_{dBs}m = -6.1497$ dBsm (frequency band in 1 to 4 GHZ), 8.021 dBsm (4 to 8 GHZ) and 8.003 dBsm (8 to 12 GHZ).
- Pressure and velocity distribution of the strike-fighter in flow field is in good condition. When the pitch angle is 3°, lift coefficient is 0.3277, drag coefficient is 0.0485 and lift-drag ratio is 6.7567.

The analysis method of conceptual design and stealth-aerodynamic characteristics of the combat aircraft can provide theoretical basis and technical support to the conceptual and stealth design of the aircraft.

ACKNOWLEDGEMENTS

This study was supported by the Natural Science Foundation of China (51375490).

REFERENCES

Anonymous (2009) Obama pledges F-22 veto as Senate gears up for aircraft fights. Defense Dail 243(9):57-62.

Baussard A, Rochdi M, Khenchaf A (2011) PO/MEC-based bistatic scattering model for complex objects over a sea surface. Eletromagnetic Waves/Progress In Electromagnetics Research (PIER) 111:229-251.

Deng H, Yu X (2013) Configuration optimization of subsonic blended wing body UAV conceptual design. Acta Aeronautica et Astronautica Sinica. 35(5): 1200 – 1208

He K, Qian W, Chen J (2009) Integrated aircraft design of aerodynamic and stealthy performance with numerically solving fluid dynamics and electro-magnetics equations. Acta Aerodynamica Sinica 27(2):180-185.

Kazuhiro N (2013) Aeronautical CFD in the age of Petaflops-scale computing: from unstructured to Cartesian meshes. Eur J Mech B Fluid 40:75-86. doi: 10.1016/j.euromechflu.2013.02.005

Peng C, Jinglong H (2012) Prediction of flutter characteristics for a transport wing with wingtip devices. Aero Sci Tech 23(1):461-468. doi: 10.1016/j.ast.2011.10.005

Rochdi M, Baussard A, Khenchaf A (2010) PO/MEC-based bistatic scattering model for complex objects over a sea surface. Proceedings of the 2010 IEEE Radar Conference; Washington, USA.

Saha S, Majumdar B (2012) Flow visualization and CFD simulation on 65° delta wing at subsonic condition. Procedia Eng 38:3086-3096. doi: 10.1016/j.proeng.2012.06.359

Scott WB (2006) B-2 program lore. Aviation Week and Space Technology 164(13):60-61.

Starosta G (2013) The F-35 readies for takeoff. Air Force Mag 96(4):38-42.

Vallespin D, Badcock KJ, Da Ronch A, White MD, Perfect P, Ghoreyshi M (2012) Computational fluid dynamics framework for aerodynamic model assessment. Progr Aero Sci 52:2-18.

Wise KA, Lavretsky E (2011) Robust and adaptive control of X-45A J-UCAS: a design trade study. Proceedings of the 18th IFAC World Congress; Milano (Italy).

Yue K, Sun C, Ji J (2014a) Numerical simulation on the stealth characteristics of twin-vertical-tails for fighter. Journal of Beijing University of Aeronautics and Astronautics 40(2):160-165.

Yue K, Sun C, Liu H (2014b) Numerical simulation on the RCS of combat aircraft for mounted missile. J Syst Eng Electron 36(1): 62-67.

Zhang H, Tan H, Li X (2009) Flow structure and performance characteristics of X-47-like slot-shaped inlet. Acta Aeronautica et Astronautica Sinica 30(12):2243-2249.